

Electronic structure of icosahedral alloys: the case of $\text{Al}_{65}\text{Cu}_{20}\text{Os}_{15}$

G.W. Zhang¹, Z.M. Stadnik¹, A.-P. Tsai², A. Inoue², T. Miyazaki³

¹ Department of Physics, University of Ottawa, Ottawa, Ontario, Canada K1N 6N5
(Fax: + 1-613/564/6712, e-mail: stadnik@acadvm1.uottawa.ca)

² Institute for Materials Research, Tohoku University, Sendai 980, Japan (Fax: + 81-22/215/2092)

³ Department of Applied Physics, Tohoku University, Sendai 980, Japan (Fax: + 81-22/224/2265)

Received: 6 September 1994

Abstract. Measurements with photoemission spectroscopy in the photon-energy range 35–130 eV have been used to determine the valence band of the stable icosahedral $\text{Al}_{65}\text{Cu}_{20}\text{Os}_{15}$. Resonant photoemission near the Os $5p \rightarrow 5d$ and $4f \rightarrow 5d$ transitions has been employed to show that the feature in the valence band with the maximum intensity at 1.5 (1) eV below the Fermi level is predominantly of the Os 5d character. This has been additionally verified by conducting the photoemission measurements in the constant-initial-state mode and by using the effect of the Cooper minimum in the photoionization cross section of the Os 5d orbitals. The valence band feature with the maximum intensity at 3.7 (1) eV below the Fermi level has been shown as being due mainly to the states of the Cu 3d character. The Os 5d and Cu 3d empirical partial density of states have been determined from the photoemission spectra. The decrease of intensity towards the Fermi level has been interpreted as being indicative of the presence of a theoretically predicted pseudogap around the Fermi level. It has been indicated, however, that the Fermi cut-off also contributes to the observed intensity decrease. It has been demonstrated that the energy resolution of the spectroscopic measurements performed so far on quasicrystals was not high enough to unambiguously determine the presence of such a pseudogap. No unusual features in the valence band of icosahedral $\text{Al}_{65}\text{Cu}_{20}\text{Os}_{15}$, which could be ascribed to its quasiperiodic nature, have been observed within the resolution of the experiment. High energy-resolution spectroscopic measurements were also shown to be essential to observe the theoretically predicted spikiness of the density of states in quasicrystals. A critical review of published spectroscopic data on the electronic structure of quasicrystals has also been presented.

PACS: 61.44. + p; 71.20. Cf; 72.15. – v; 79.60. – i

1. Introduction

The discovery of an icosahedral Al-Mn alloy by Shechtman et al. [1] extended the dichotomous division of solids

into either crystalline or amorphous by introducing the notion of quasiperiodic crystals, or quasicrystals (QCs) for short. This new form of matter possesses long-range *quasiperiodic* order and long-range orientational order associated with the classically forbidden five-fold, eight-fold, ten-fold, and 12-fold symmetry axes [2, 3]. A central problem in condensed-matter physics is to determine how quasiperiodicity affects various physical properties of a material, and its electronic structure in particular. A comprehensive understanding of the physical properties of QCs is ultimately dependent upon knowledge and understanding of their electronic structure.

The first few years of studies of QCs revealed that their physical properties are similar to either corresponding crystalline or amorphous counterparts [4]. It was only later realized that the first QCs, which were thermodynamically *metastable*, possessed significant structural disorder, as manifested in the broadening of the X-ray- or electron-diffraction lines. They also contained non-negligible amounts of second phases. These poor quality samples hampered the detection of those properties which were intrinsic to quasiperiodicity. They also led to confusion, especially in the area of the magnetic properties of QCs where some “unusual” magnetic properties were claimed to have been observed [5]. Some of these properties were later shown [6, 7] to result from the presence of magnetic second phases in the studied *icosahedral*-alloys.

New opportunities for experimental studies of QCs arose when the thermodynamically *stable* icosahedral (*i*) alloys Al-Cu-(Fe, Ru, Os) [8, 9] and Al-Pd-(Mn, Re) [10, 11] were discovered because these stable QCs possess a high degree of structural perfection comparable to that found in the best periodic alloys. These stable *i*-alloys exhibit some unexpected behaviour. Their most salient feature, which is not expected for alloys formed of normal metallic elements, is the very high value of the electrical resistivity [2–4] (up to the record high value of about $2.0 \Omega \cdot \text{cm}$ at 4.2 K in *i*-Al-Pd-Re alloys [12]). This corresponds to an electrical conductivity [4, 12] comparable to or smaller than the Mott’s “minimum metallic conductivity” of $200 \Omega^{-1} \cdot \text{cm}^{-1}$ for the metal-insulator transition [13]. It was even suggested [14] that *i*-Al-Pd-Re alloys are

in fact quasiperiodic insulators. The resistivity of these new *i*-alloys increases as their structural quality improves (by annealing which removes the defects [15, 16]), in contrast to the behaviour of typical metals. Additionally, the resistivity is extremely sensitive to sample composition [12, 15, 16], which is reminiscent of doping effects in semiconductors in which large changes of resistivity result from small amounts of appropriate impurities. The temperature coefficient of resistivity is generally negative [4, 12, 15, 16], which is inconsistent with the expected behaviour for metals. Other anomalies in the transport properties of QCs involve the very low electronic contribution to the specific heat, large and strongly temperature-dependent Hall coefficients and thermoelectric power, and a non-Drude-like optical conductivity [2–4, 12, 14–16]. From a magnetic point of view, the stable *i* alloys Al-Cu-Fe and Al-Pd-Mn of high structural quality are unusual in that they are diamagnetic in spite of containing significant concentrations of Fe and Mn [15, 17].

The electronic transport properties of QCs mentioned above have been interpreted using several models, none of which is yet firmly established. By far the most commonly invoked model is the one based on a Hume-Rothery effect. It was pointed out by Hume-Rothery in 1926 [18] that certain metallic alloys, which are now called the Hume-Rothery or electron phases, are stable at well defined values of the number of valence electrons per atom. It was later shown by Mott and Jones [19] via a simple electronic theory of metals that for these critical values the Fermi sphere of radius k_F just touches the Brillouin zone plane, which corresponds to the relation $Q = 2k_F$, where Q is the magnitude of the reciprocal lattice vector. Such a Fermi surface-Brillouin zone interaction opens an energy gap at the Fermi surface, which results in the minimum in the density of states (DOS) at the Fermi level E_F . It has been argued that the very low values of the electrical conductivity and of the electronic contribution to the specific heat in stable QCs indicate very low values of the DOS (E_F) [4]. This experimental fact was often taken as evidence for the existence of a minimum (a pseudogap) in the DOS (E_F) in QCs [4]. Apart from its simplicity, expressed in the relation $q = 2k_F$, the Hume-Rothery mechanism is so appealing because one can explain qualitatively why the stable QCs possess the lowest values of the electrical conductivity and the low electronic contribution to the specific heat. It can be also used to explain why stable QCs can exist only in a rather narrow composition range (a small composition change can shift the E_F from the DOS minimum). It should be emphasized, however, that such a widespread and enthusiastic application of the Hume-Rothery mechanism to QCs is open to criticism [20]. The original Hume-Rothery mechanism [18, 19] was suggested for alloys with the *sp* valence electrons. Applying it to quasicrystalline systems with *d* electrons may be unjustified. Furthermore, it is not clear what is understood by the Brillouin zone in a quasicrystalline alloy for which one cannot define a unique unit cell. And finally, as critically reviewed in the literature [21], the apparent correlation between the number of valence electrons per atom and a special structural stability is the exception rather than the rule in crystalline systems, and

the Mott-Jones [19] interpretation of the Hume-Rothery mechanism, which associates a special stability with the Brillouin zone faces touching the Fermi sphere, is simply incorrect in general.

The notion of a structure-induced pseudogap in the DOS around E_F in QCs seems to be supported by theory based on a nearly-free-electron approximation [22–26] and by electronic structure calculations performed for the lowest-order crystalline approximants [27–32]. As has been noted by Hafner and Krajčí [32], although the structure-induced pseudogap at the Fermi level seems to be a *generic* property of QCs, it is not a *specific* property distinguishing the quasiperiodic from the periodic or aperiodic phases because it is also present in some amorphous and crystalline alloys. This is supported by recent NMR results [33] which show low values of DOS (E_F) in both *i*-alloys and their crystalline approximants. According to some electronic structure calculations done for the lowest-order approximants [27–30], the specific property of QCs seems to be the spikiness of their DOS, resulting from a large number of non-degenerated flat bands. Such DOS spikiness does not occur in crystalline or amorphous systems.

A possible existence of a pseudogap in the DOS around E_F may be not the only reason of the unusual electronic transport properties of stable QCs. There are two other mechanisms which have been recently proposed in the literature. The first one, which is very qualitative in nature, is based on an internal structural model which assumes the presence of conductive *i*-blocks which are surrounded by an insulating layered-structure network [34, 35]. In this structural model the electrical conduction occurs via tunnelling which may explain qualitatively many of the electronic transport characteristics of QCs. The second mechanism is the intraband transition mechanism [29, 36, 37] which invokes the concepts of localization and critical states.

The electrical conductivity of stable *i*-alloys in the low temperature range has a characteristic temperature dependence: it is proportional to \sqrt{T} for the lowest temperatures and to T at higher temperatures [2–4, 38]. These temperature dependencies, as well as those of magnetoresistance, are usually explained using quantum interference theories (the electron–electron interaction and weak-localization effects) [2–4, 38]. Such theories, however, were originally developed for highly disordered conductors. Thus, their apparent relevance to stable *i*-alloys indicates that these alloys are electronically disordered. This, however, poses a question: how can such electronic disorder be reconciled with the apparent high degree of local atomic order in stable *i*-alloys, as determined by diffraction and electron-microscopy experiments? We shall present some plausible reasons of this apparent contradiction in section 3E of this paper. In summary, at present a full understanding of the unusual electronic transport properties of QCs remains elusive.

The electronic transport measurements reviewed above have made an important contribution to our understanding of the electronic structure of QCs. It should be stressed, however, that these measurements provide *indirect* information on the DOS at one particular energy (E_F). To determine the electronic structure of QCs one

needs information not only on the DOS (E_F), but also on the DOS below and above E_F . Therefore, studies using spectroscopic techniques which probe DOS *directly* at energies in the vicinity of E_F are very desirable. X-ray photoelectron spectroscopy (XPS), photoemission spectroscopy (PES), and soft X-ray emission (SXE) spectroscopy have been employed to study the DOS below E_F , whereas the DOS above E_F was probed with the inverse photoemission spectroscopy (IPES) and soft X-ray absorption (SXA) spectroscopy in Al-Mn-Si, Al-Li-Cu-Mg, Al-Cu-Fe(Cr), Al-Cu-Ru, Al-Pd-Mn, Al-Ga-Mg-Zn, Al-Cu-Mn, and Al-Pd-Mg QCs [39–55]. These electronic structure studies lead to several conclusions, which will be discussed in detail in Sect. 3 in relation to the present study, and which are briefly summarized below. First, the most important finding is the apparent observation in some QCs of the pseudogap at E_F , which is predicted by theory and suggested by the results of electronic transport measurements. However, an unambiguous spectroscopic verification of the existence of such a pseudogap for QCs containing the transition-metal (TM) elements is very difficult because the experimentally measured intensity in the vicinity of E_F is dominated by the TM 3d states, as is well known from similar studies of the structurally induced minimum in the DOS in amorphous alloys [56]. We shall argue in section 3D that the unambiguous spectroscopic verification of the possible existence of such a pseudogap requires much better energy resolution than that used until now. Second, chemical shifts of the Al 2p lines are either zero or very small with respect to similar crystalline compounds or pure elements. This disagrees with the theoretical result [5, 57] which predicts large shifts and thus confirms the conclusion of recent theoretical studies [58] of the unreliability of predictions [5, 57] based on calculations performed on small clusters. Third, a close structural similarity between the valence-band spectra of QCs and those of the corresponding crystalline compounds was found. No spikiness in the DOS of QCs predicted by the theory was observed. Finally, various measured spectral features were ascribed to particular electronic states of *s*, *p*, and *d* character, and some arguments for the hybridization between sp and d states were presented.

For the family of stable Al-Cu-(Fe,Ru,Os) *i*-alloys, almost all physical measurements have so far been performed on the Al-Cu-Fe and Al-Cu-Ru alloys. Apart from a few structural investigations of the Al-Cu-Os *i*-alloys [9, 59, 60], we are aware of only one experimental paper [61] in which the ^{27}Al and ^{63}Cu NMR spectra of *i*-Al_{6.5}Cu_{2.0}Os_{1.5} were presented. This is rather surprising in view of the high structural quality of the stable *i*-Al_{6.5}Cu_{2.0}Os_{1.5} alloy [59, 60, 62].

This paper reports the first study of the electronic structure of a high-quality *i*-Al_{6.5}Cu_{2.0}Os_{1.5} alloy using the synchrotron-radiation-based PES technique. By employing the photon-energy dependence of the photoionization cross section and the effect of a core-electron resonance, we are able not only to identify the origin of the prominent features in the valence band of the studied alloy, but also to separate the overlapping contributions due to the Cu 3d and Os 5d states. Before the emergence of the synchrotron-radiation-based PES technique, such a sep-

aration of contributions of a given symmetry (*s*, *p*, *d*, or *f*) due to a specific element could be only obtained from the SXE technique. A critical review of the published spectroscopic evidence for the existence of a pseudogap at the Fermi energy, as well as a discussion of the problem of the DOS spikiness in stable QCs are presented.

2. Experimental procedure

An alloy of composition Al_{6.5}Cu_{2.0}Os_{1.5} was produced by arc melting high-purity elemental constituents in argon. It was annealed at 1173 K for 48 h in vacuum, and then cut into slices suitable for PES measurements. The details of the sample preparation are described elsewhere [9]. The X-ray diffraction study showed [62] that the samples are single phase and exhibit resolution-limited Bragg-peak widths.

Photoemission spectra were collected on beamline U14A at the National Synchrotron Light Source at the Brookhaven National Laboratory. Photon energies between 35 and 130 eV were selected with a plane grating monochromator. The normal to the sample was at an angle of 45° to both the photon beam and the axis of a PHI 15–255 precision electron energy analyzer. The resulting overall resolution obtained by fitting the Fermi edge of each spectrum to a Fermi-Dirac distribution (at room temperature) convolved with a Gaussian was about 0.4 eV. The sample was cleaned in the experimental vacuum chamber either by 1.5-keV Ar⁺ bombardment for a few minutes or by gentle mechanical abrasion using an alumina scraper. No differences between the PES spectra corresponding to these two surface-treatment methods could be detected. The surface cleanliness of the sample was frequently checked by monitoring the appearance of the oxide features in the Al 2p line and/or in the valence band [48]. The base pressure in the experimental chamber was in the high 10⁻¹¹ Torr range.

All the spectra presented in this work were obtained from at least two different regions of the same sample studied, and turned out to be indistinguishable within the resolution of the experiment. The position of the Fermi level was determined by measuring the Fermi edge and/or the Al 2p line (for photon energies larger than 100 eV) of an adjacent Al sample. It was additionally verified by a fit of the leading edge of the valence band of the measured spectra to a Fermi-Dirac distribution convolved with a Gaussian.

3. Results and discussion

A. Methodology of evaluation of the raw photoemission spectra

In order to compare the intensities of the synchrotron-radiation-based PES spectra of a given sample, several corrections have to be taken into account [50]. First, all our PES spectra presented here were corrected for the energy dependence of the electron transmission of the electron energy analyzer. It was assumed that the transmission of the analyzer, including the retarding lens

system, is inversely proportional to the kinetic energy of the electrons [63]. Next, the PES spectra were normalized to the time dependent photon-flux. The secondary-electron contribution was then subtracted by using the Shirley method [64] in which the secondary-electron background intensity at each binding energy (BE) is assumed to be proportional to the total integrated signal at lower binding energies. The first two corrections slightly modify the shape of the original spectrum, whereas the subtraction of the secondary-electron contribution causes the largest changes (Fig. 1). These corrections have no significant influence on the shape of the spectrum close to E_F , but modify the spectrum substantially at higher binding energies (the negative value of BE in Fig. 1 indicates the energy scale below E_F). The PES spectra corrected in such a way can be compared not only with respect to their shape but also in terms of their intensities. This is especially important when the intensity scale of the PES spectra is used, as is the case in this paper, to obtain information on various features of the valence bands and on the partial DOS due to a specific element in an alloy.

B. Structure of the valence band

The structure of the valence band of $i\text{-Al}_{65}\text{Cu}_{20}\text{Os}_{15}$ (Fig. 1) consists of two overlapping peaks and a broad and weak spectral weight around $\text{BE} = -6$ eV. The two peaks must be predominantly due to the Os 5d and the Cu 3d states because the Al sp spectral contribution is expected to be much smaller due to the small photoionization cross section, σ , for Al sp orbitals for the photon energies used here (Fig. 2) [65]. In order to identify unambiguously the origin of these two features, photoemission spectra were measured at different photon energies.

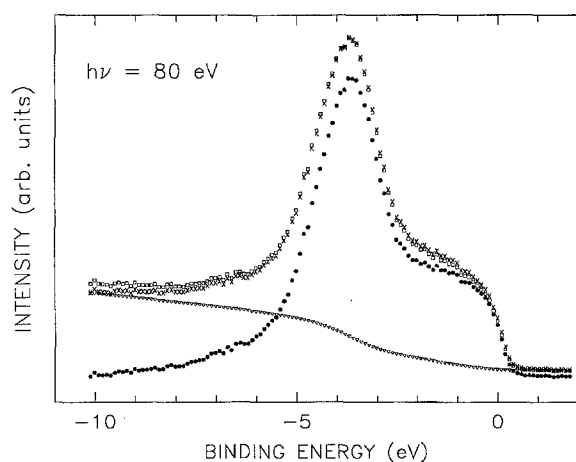


Fig. 1. Effect of the secondary-electron contribution on the valence-band spectrum of $i\text{-Al}_{65}\text{Cu}_{20}\text{Os}_{15}$ measured at a photon energy $h\nu = 80$ eV. (□) – the as-measured spectrum, (×) – the analyzer- and flux-corrected as-measured spectrum scaled to the most intense peak of the as-measured spectrum, (▽) – secondary-electron contribution to the analyzer- and flux-corrected as-measured spectrum, (●) – resultant spectrum after subtraction of the secondary-electron contribution

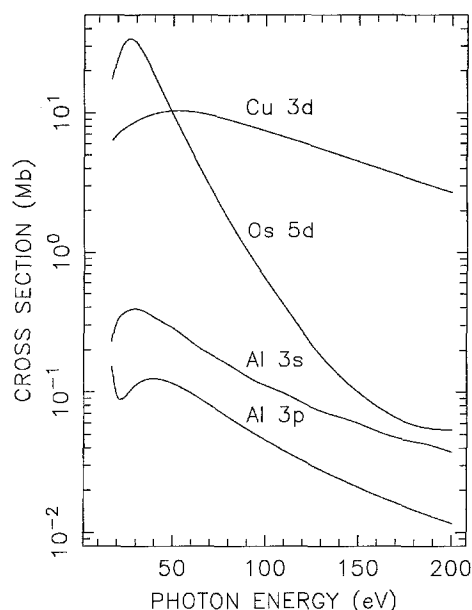


Fig. 2 Atomic subshell photoionization cross sections as a function of photon energy for Cu 3d, Os 5d, Al 3s, and Al 3p orbitals. Data are taken from [65]. Note the logarithmic scale on the ordinate axis

B1. Resonant photoemission data. To determine the main features in a valence band due to the Os 5d states, the resonant photoemission can be employed [66]. In this effect the ionization cross section of an outer-shell electron increases when the excitation energy exceeds the threshold of an inner excitation. For TM elements the resonance occurs at excitation energies near the np and nf thresholds. For an Os metal one would expect the stronger $5p \rightarrow 5d$ transition to occur at about 44.5 eV ($5p_{3/2} \rightarrow 5d$) and the weaker $4f \rightarrow 5d$ transition to take place at about 50.7 eV ($4f_{7/2} \rightarrow 5d$) [67]. The Os 5d-derived features should be enhanced or suppressed [66] as the photon energy is swept through the $5p$ - $5d$ and $4f$ - $5d$ thresholds. It can be seen in Fig. 3 that, as the photon energy increases, the relative intensity of the peak at about $\text{BE} = -1.5$ eV with respect to the peak at about $\text{BE} = -3.7$ eV decreases first and reaches its minimum at $h\nu = 44.5$ eV. Then it increases slightly between $h\nu = 50$ and 60 eV. This corresponds to the stronger $5p \rightarrow 5d$ resonance (the $4f \rightarrow 5d$ resonance is too weak to be observed in the measured valence bands) and thus indicates that the peak at about $\text{BE} = -1.5$ eV is predominantly due to the Os 5d-derived states. It should be noted that the $5p \rightarrow 5d$ and $4f \rightarrow 5d$ resonances occur in the photon energy region where there is a strong decrease of σ (Os 5d) (Fig. 2), and consequently the decrease of the relative intensity of the peak at $\text{BE} = -1.5$ eV is due not only to the stronger $5p \rightarrow 5d$ resonance, but also due to the decrease of σ (Os 5d). Nevertheless the decrease of the relative intensity of the $\text{BE} = -1.5$ eV peak when going from $h\nu = 40$ eV to 44.5 eV (Fig. 3) is stronger than expected only from the σ changes (Fig. 2), and supports the conclusion that the intensity change is mainly due to the Os $5p \rightarrow 5d$ resonance, and thus the feature at $\text{BE} = -1.5$ eV is predominantly due to Os 5d-derived states. It is worth indicating here that the σ values presented in Fig. 2 are the *atomic*

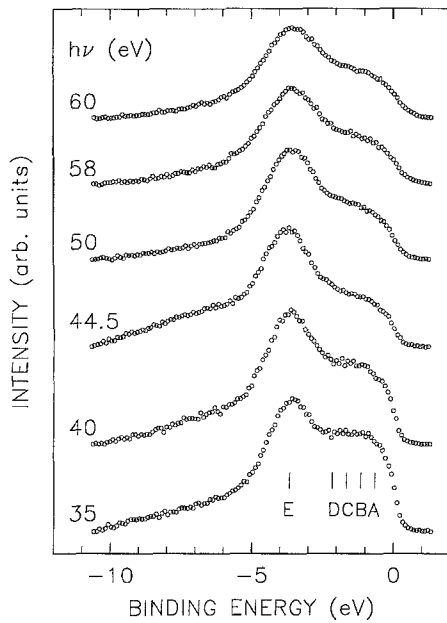


Fig. 3 Valence-band spectra of $i\text{-Al}_{65}\text{Cu}_{20}\text{Os}_{15}$ for different photon energies around the Os $5p \rightarrow 5d$ transition. A, B, C, D, and E identify binding energies for which CIS spectra were measured (Fig. 4)

values [65] and are expected to be different in elemental metals and their alloys. In fact, it is well established experimentally [68] that, due to solid-state effects, σ values in metallic systems differ significantly from the atomic values [65]. Nevertheless, the trends in the $\sigma(h\nu)$ are similar in metallic systems [68] to those in the corresponding atomic systems [65]. Therefore, in view of the lack of calculations of the σ values in the metallic alloys, the calculated atomic σ values are very useful in interpreting the PES data.

Another way of performing a photoemission experiment, which shows more clearly the resonant photoemission intensity variations, is to measure the so-called constant-initial-state (CIS) spectra [69]. These spectra represent the dependence of the photoemission intensity on the photon energies for selected valence-band positions which are identified by their initial energy E_i . Such CIS spectra for the E_i values corresponding to the positions denoted by A, B, C, D, and E in Fig. 3 are shown in Fig. 4. One can see a minimum for photon energies around 44 eV, and another weak minimum for photon energies around 51 eV. The resonance line shape, $I(h\nu)$, can be characterized by the Fano profile [69]

$$I(h\nu) = I_0(h\nu) \frac{(\varepsilon + q)^2}{1 + \varepsilon^2} + I_{nr}(h\nu), \quad (1)$$

where $I_0(h\nu)$ is the nonresonant Os $5d$ emission, $I_{nr}(h\nu)$ is a noninterfering background contribution, q is Fano's asymmetry parameter, and $\varepsilon = 2(h\nu - E_R)/\Gamma$ is the reduced energy expressed in terms of the energy, E_R , and the width, Γ (FWHM), of the resonance. The experimental CIS spectra (Fig. 4) were fitted to two Fano profiles in order to account for the two Os $5p \rightarrow 5d$ and $4f \rightarrow 5d$ transitions mentioned above. A linear background I_{nr} was

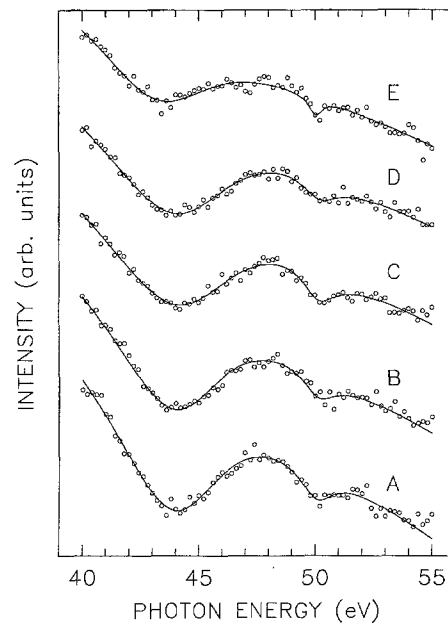


Fig. 4 Constant-initial-state (CIS) spectra measured for the valence-band positions A, B, C, D, and E in Fig. 3, which are identified here by the same letters. The raw CIS spectra were corrected for the energy dependence of the electron transmission for the analyzer and for the time-dependent photon flux. The solid line is a fit to two Fano profiles and a linear background, as described in the text and with parameters given in Table 1

assumed in the fit. The parameters obtained from the fit are given in Table 1.

Even though a good fit was obtained (Fig. 4) with the two Fano profiles described above, the fitted parameters are correlated due to the overlap of two broad $5p_{3/2} \rightarrow 5d$ and $4f_{7/2} \rightarrow 5d$ transitions, and therefore caution is required in their physical interpretation. As expected, the nonresonant emission parameters corresponding to the two transitions fulfil the inequality $I_0^{3/2} > I_0^{7/2}$ (Table 1). The resonance energies $E_R^{3/2}$ and $E_R^{7/2}$ (Table 1) are close to the corresponding core-level values for an Os metal. The broad character of the resonance is reflected (Table 1) in the large values of Γ . The strongest resonance occurs for $E_i = -1.7$ eV (Fig. 4 and Table 1), and the weaker resonances can be also observed both below and above the $E_i = -1.7$ eV value. The fact that the resonance takes place in a rather broad valence band region can be interpreted as evidence of hybridization between the Os $5d$ and the Al $3p$ and/or Cu $3d$ states.

B2. Photoemission data near the Cooper minimum. The features in the valence bands originating from the $4d$ and/or $5d$ states in alloys containing the $4d$ and/or $5d$ elements can be identified by making use of the Cooper minimum effect [68] which is the occurrence of a minimum in the σ values for particular orbitals at a specific photon energy. This effect results from the presence of one or more nodes in the radial part of the $4d$ and $5d$ (but not $3d$) atomic wave functions. The Cooper minimum in the σ (Os $5d$) is calculated to be at about $h\nu = 200$ eV for an Os atom [65] (Fig. 2). However, its position and depth are expected to be changed in alloys due to solid-state effects

Table 1. Parameters obtained by fitting the CIS spectra in Fig. 4, for the E_i values corresponding to the positions A, B, C, D, and E indicated in Fig. 3, to two Fano line shapes (Eq. 1) associated with the Os $5p_{3/2} \rightarrow 5d$ and $4f_{7/2} \rightarrow 5d$ transitions. The parameters with the superscripts 3/2 and 7/2 refer respectively to the Os $5p_{3/2} \rightarrow 5d$ and $4f_{7/2} \rightarrow 5d$ transitions

| Label | E_i (eV) | $I_0^{3/2}$ | $I_0^{7/2}$ | $E_R^{3/2}$ (eV) | $E_R^{7/2}$ (eV) | $q^{3/2}$ | $q^{7/2}$ | $\Gamma^{3/2}$ (eV) | $\Gamma^{7/2}$ (eV) |
|-------|------------|-------------|-------------|------------------|------------------|-----------|-----------|---------------------|---------------------|
| A | -0.67 | 155(11) | 36(5) | 44.3(2) | 50.1(2) | 0.24(6) | 0.01(17) | 6.0(5) | 1.8(4) |
| B | -1.17 | 188(18) | 40(8) | 44.3(2) | 50.0(3) | 0.24(6) | -0.12(20) | 6.1(7) | 1.8(6) |
| C | -1.67 | 193(19) | 52(8) | 44.6(3) | 50.0(2) | 0.29(8) | -0.20(15) | 7.2(8) | 1.8(4) |
| D | -2.17 | 187(19) | 37(6) | 44.4(2) | 50.0(6) | 0.27(6) | -0.16(8) | 7.1(8) | 1.9(5) |
| E | -3.67 | 136(19) | 30(7) | 43.4(9) | 50.0(2) | 0.14(7) | 0.01(20) | 6.2(9) | 0.7(3) |

[50, 68]. Usually, the shift is by about 30 eV towards higher $h\nu$ values and the minimum is shallower [50, 68] than predicted by atomic calculations [65]. Since the decrease of the σ (Os 5d) in the 50 to 200 eV photon energy range is expected to be about two orders of magnitude (Fig. 2), one can anticipate a strong suppression of the contribution of the Os 5d character to the valence band of $i\text{-Al}_{65}\text{Cu}_{20}\text{Os}_{15}$ for values of $h\nu$ close to the Cooper minimum.

Figure 5 shows that as $h\nu$ increases from 80 eV, the relative contribution of the first feature with the peak at $\text{BE} \approx -1.5$ eV with respect to the other feature with the peak at $\text{BE} \approx -3.7$ eV, which originates from the Cu 3d-derived states, decreases steadily and at $h\nu = 130$ eV is almost completely suppressed. In other words, since σ (Cu 3d) decreases much slower with the increase of $h\nu$ than does σ (Os 5d) (Fig. 2), and since σ (Cu 3d) for $h\nu = 130$ eV is expected to be almost two orders of magnitude larger than σ (Os 5d) (Fig. 2), the $h\nu = 130$ eV valence band (Fig. 5) must be almost entirely due to the Cu 3d emission. It is worth noting that the Cooper minimum effect is much more dramatic (Fig. 5) than the Os $5p \rightarrow 5d$ photoemission resonance effect (Fig. 3).

To show the effect of the Cooper minimum in a more quantitative way, a plot of the photoemission intensity at $\text{BE} = -1.5$ eV as a function of the $h\nu$ is presented in Fig. 6. This intensity was obtained as an average of 11 intensity values around $\text{BE} = -1.5$ eV. One can see clearly a strong decrease of the photoemission intensity with increasing photon energy. However, this decrease is not by about an order of magnitude, as expected from Fig. 2, but by about the factor of five. As mentioned above, this is caused by solid-state effects [50, 68]. However, the trend in the σ (Os 5d) dependence on $h\nu$ in the studied alloy (Fig. 12) is similar to that based on atomic calculations (Fig. 2). The contribution due to the Cu 3d-like states is well separated at $h\nu = 130$ eV from the contribution originating from the Os 5d-like states (Fig. 5) and has its peak at $\text{BE} = -3.7(1)$ eV. The weak and broad spectral weight around $\text{BE} = -6$ eV (Figs. 3 and 5) can be ascribed to the Al sp-derived states, based on the results of SXE studies of $i\text{-Al}$ -based alloys [51].

It is now widely accepted that PES valence bands measured typically for $h\nu \geq 40$ eV (XPS regime) represent the initial DOS weighted by frequency-dependent dipole matrix elements and by the $\sigma(h\nu)$ values for various s, p, d, and f states [70]. To a good approximation, it can be assumed that the matrix elements change little over the width of the valence band. Thus the measured PES valence bands, when properly corrected for experimental

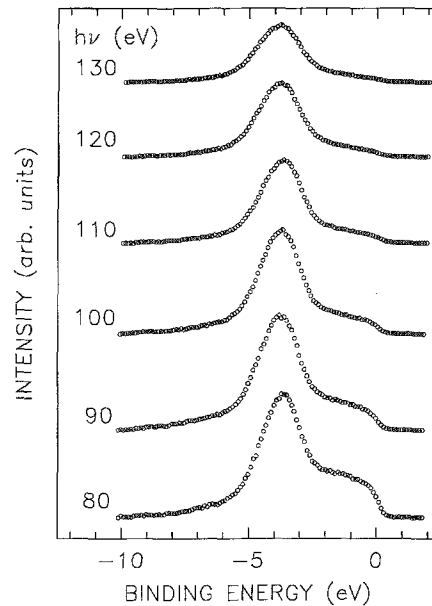


Fig. 5. Valence-band spectra of $i\text{-Al}_{65}\text{Cu}_{20}\text{Os}_{15}$ for different photon energies around the Os 5d Cooper minimum

factors and for inelasticity scattered electrons, are generally proportional to the DOS modulated by the photoionization cross sections. In the particular case of $i\text{-Al}_{65}\text{Cu}_{20}\text{Os}_{15}$, the valence bands measured for $h\nu$ values which are outside the Os $5p \rightarrow 5d$ resonance and for which σ (Cu 3d) \approx σ (Os 5d), are expected to well represent the total DOS of the d character. Since σ (Cu 3d) \approx σ (Os 5d) occurs at around $h\nu = 50$ eV (Fig. 2), the valence bands measured in the vicinity of that photon energy should represent well the total d-derived DOS in the studied alloy. Additional arguments in support of this statement will be given below.

C. Partial DOS due to Os 5d- and Cu 3d-derived states

The analysis presented above made it possible to unambiguously ascribe the two main features in the valence band of $i\text{-Al}_{65}\text{Cu}_{20}\text{Os}_{15}$ to the Os 5d- and Cu 3d-derived states. To determine the experimental electronic structure associated with the occupied energy levels of an alloy, it is also necessary to establish partial spectral weights due to s, p, d, and f states of a given element in the alloy. These partial weights are generally proportional to the partial DOS associated with a given state of that element, as was

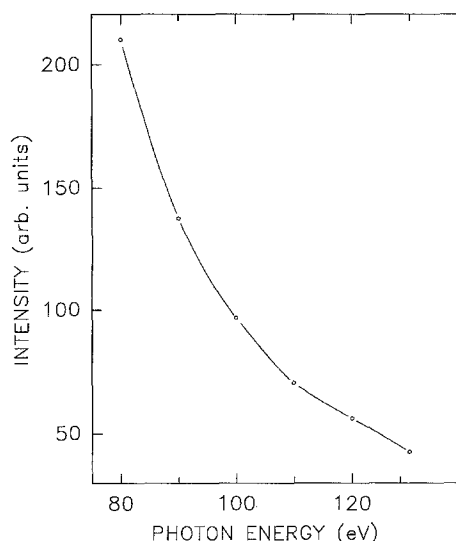


Fig. 6. Photoemission intensity at the binding energy of -1.5 eV as a function of photon energy obtained from the spectra in Fig. 5, as described in the text. The solid line is a guide for the eye

discussed above. Before the advent of synchrotron radiation as a tunable excitation source, such partial DOS was determined almost exclusively using the SXE technique. The use of synchrotron-radiation-based PES technique allows one also to determine the partial DOS for some orbitals, as is demonstrated below.

PES valence bands represent mainly the DOS of orbitals with d and/or f character because the σ values corresponding to these orbitals are significantly larger than the values associated with the s and p orbitals ([65] and Fig. 2). Thus, to a first approximation, the contribution to the valence band of $i\text{-Al}_{65}\text{Cu}_{20}\text{Os}_{15}$ from sp states can be neglected. The intensity $I(h\nu, \text{BE})$ of the valence band PES spectrum of $i\text{-Al}_{65}\text{Cu}_{20}\text{Os}_{15}$ at a binding energy BE and at an incident photon energy $h\nu$ can be represented [71] by

$$I(h\nu, \text{BE}) = C(h\nu) [\sigma_{\text{Cu}}(h\nu) D_{\text{Cu}}(\text{BE}) / Z_{\text{Cu}} + \sigma_{\text{Os}}(h\nu) D_{\text{Os}}(\text{BE}) / Z_{\text{Os}}], \quad (2)$$

where D_i is the partial DOS of the i -th element ($i = \text{Cu}, \text{Os}$). The partial DOS is assumed to fulfil the normalization condition

$$\sum D_i(\text{BE}) \Delta \text{BE} = N_i Z_i, \quad (3)$$

where N_i and Z_i are respectively the concentration and the number of d electrons of the i -th element. Here $N_{\text{Cu}} = 20$, $N_{\text{Os}} = 15$, and we assume that $Z_{\text{Cu}} = 10$ and $Z_{\text{Os}} = 6$. The instrumental factor is represented by $C(h\nu)$. In principle, this factor should be independent of $h\nu$ if the corrections to the as-measured valence bands, which are described in Sect. 3A, could be done ideally and if one could know precisely the values of $\sigma_{\text{Cu}}(h\nu)$ and $\sigma_{\text{Os}}(h\nu)$ in the studied alloy. Since in practice this cannot be achieved, the factor $C(h\nu)$ has a weak dependence on $h\nu$.

For compounds containing a d - or f -electron element for which a Cooper minimum or resonance photoemission effects can be observed, it has been standard practice to use the difference between the valence bands away from

and at the Cooper minimum [68, 72], or between the on- and off-resonance valence bands [72, 73], to determine the partial DOS of that element. Such a difference spectrum enhances the d or f contribution of that element to the valence band because of the strong variation of the d - and f -like spectral weights for $h\nu$ values close to the values at which Cooper minima or resonance photoemission occur, and because the changes of the σ values with $h\nu$ of the orbitals of other elements of an alloy are usually negligibly small, and thus cancel out. Since the Cooper minimum effect has a much more pronounced influence on the intensity changes in a valence band than the resonance effect, we used the former to derive the Os 5d and Cu 3d partial DOS from the PES spectra.

In order to assess the reliability and the reproducibility of the Os 5d and Cu 3d partial DOS in $i\text{-Al}_{65}\text{Cu}_{20}\text{Os}_{15}$ which were obtained from the PES spectra, two approaches were used. In the first approach, a difference spectrum was obtained by direct subtraction of the $h\nu = 90$ eV spectrum from the $h\nu = 80$ eV spectrum of Fig. 5 (triangle symbols in Fig. 7). It represents the Os 5d partial DOS because the small change of $\sigma(\text{Cu } 3d)$ in the $h\nu$ range 80–90 eV (Fig. 2) assures that the Cu 3d contribution effectively cancels out in the difference spectrum. Note that the direct subtraction is equivalent to the assumption that $C(h\nu)$ and $\sigma_{\text{Cu}}(h\nu)$ in (2) are independent of $h\nu$ which, as indicated above, is justified to a first approximation. Next, the difference between the same valence-band spectra was calculated as $I(90 \text{ eV}) - h_{\text{Os}} I(80 \text{ eV})$ by scaling the $h\nu = 80$ eV spectrum by the factor $h_{\text{Os}} = 0.61$ to match the height of its Os 5d feature to that of the $h\nu = 90$ eV spectrum (curve marked with open circle symbols in Fig. 7); this is a graphical attempt to account for the differences between the $\sigma_{\text{Os}}(h\nu)$ values at $h\nu = 80$ eV and $h\nu = 90$ eV. This procedure assures that the Os 5d contribution cancels out in the difference spectrum which thus represents the Cu 3d partial DOS. The total

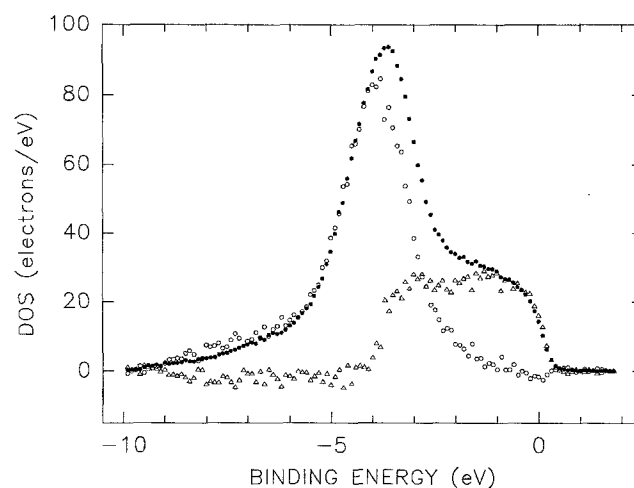


Fig. 7. Differences between the $h\nu = 80$ eV and $h\nu = 90$ eV spectra from Fig. 5 obtained by a direct subtraction (Δ), and by a subtraction following the scaling to the Os 5d features of the two spectra (\circ), as described in the text. They represent respectively the Os 5d and Cu 3d partial DOS. The sum (\bullet) of the difference spectra represents the total DOS of the d -character in $i\text{-Al}_{65}\text{Cu}_{20}\text{Os}_{15}$

d -derived DOS is shown by the filled circle symbols in Fig. 7. All the three DOS plots in Fig. 7 fulfil the normalization condition of (3). This method applied to other valence bands in the vicinity of the Os 5d Cooper minimum leads to essentially the same Os 5d and Cu 3d partial DOS as those shown in Fig. 7.

The second approach of obtaining the Cu 3d and Os 5d partial DOS from the measured valence bands is based on using (2) for two different $h\nu$ values. The factors $C(h\nu)$ corresponding to these values are then determined from the total integrated intensity of the experimental valence bands, the normalization condition of (3), and the values of $\sigma_{\text{Cu}}(h\nu)$ and $\sigma_{\text{Os}}(h\nu)$. Because of the expected shift of the Cooper minimum by about 30 eV towards higher $h\nu$ values in the studied alloy, which was mentioned earlier, the modified $\sigma_{\text{Os}}(h\nu)$ values corresponding to the atomic values $\sigma_{\text{Os}}(h\nu - 30)$ were used [65]. The Cu 3d and Os 5d partial DOS obtained in this way by using the $h\nu = 80$ eV and $h\nu = 130$ eV valence bands from Fig. 5, as well as their sum, are shown in Fig. 8. It should be stressed that essentially the same results as those in Fig. 8 are obtained for other pairs of measured valence bands. As can be seen by comparing Figs. 7 and 8, the Cu 3d and Os 5d partial DOS obtained by the two methods are very similar, which gives us confidence in their reliability.

By using (2), one should be able to reproduce the experimental valence bands measured for all $h\nu$ values provided that the Cu 3d and Os 5d partial DOS in Fig. 8 are a good measure of the true Cu 3d and Os 5d DOS in $i\text{-Al}_{65}\text{Cu}_{20}\text{Os}_{15}$ and provided that the used $\sigma_{\text{Cu}}(h\nu)$ and $\sigma_{\text{Os}}(h\nu)$ values are accurate enough. The reproduced valence bands calculated for all $h\nu$ values are compared with the corresponding experimental valence bands in Fig. 9. Obviously, a perfect agreement (Fig. 9) between the experimental valence bands measured at $h\nu = 80$ eV and $h\nu = 130$ eV and the corresponding generated bands occurs because these two experimental valence bands were used to determine the Cu 3d and Os 5d partial DOS in Fig. 8. Keeping in mind the simplicity of the model expressed by (2), there is a good agreement between the predictions of the model and the experimental data (Fig. 9).

D. Minimum of $\text{DOS}(E_F)$ and DOS spikiness in quasicrystals

It would be desirable to compare the valence band of $i\text{-Al}_{65}\text{Cu}_{20}\text{Os}_{15}$ with that of a corresponding crystalline alloy. Unfortunately, no ternary Al-Cu-Os alloys are known. Consequently, no theoretical calculations of the DOS in an approximant of the $i\text{-Al}_{65}\text{Cu}_{20}\text{Os}_{15}$ alloy can be performed. Thus, we cannot compare our empirically determined DOS and the Cu 3d and Os 5d partial DOS (Fig. 8) with theory. We therefore compare the valence band of $i\text{-Al}_{65}\text{Cu}_{20}\text{Os}_{15}$ with the valence bands of its constituent elements (Fig. 10). One can notice (Fig. 10) a clear shift of the Cu 3d spectral weight in the studied alloy away from E_F as compared with the corresponding spectral weight in pure Cu. Such a shift is expected to result in a decrease of the Cu 3d contribution to the $\text{DOS}(E_F)$. A similar shift is not observed for the Os 5d spectral weight (Fig. 10) and consequently one can anti-

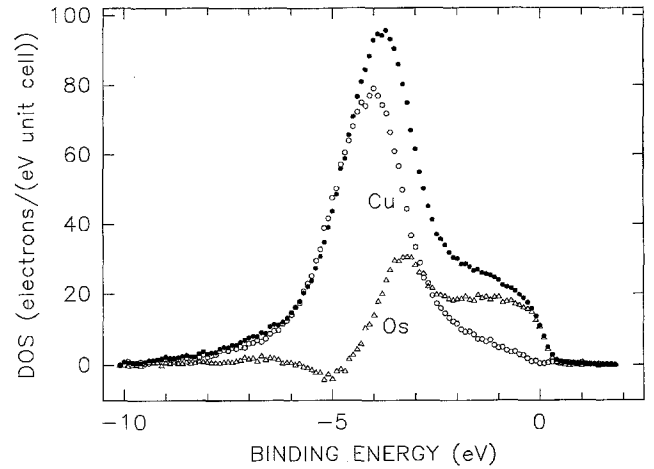


Fig. 8. Partial DOS of the Os 5d-derived states (Δ) and the Cu 3d-derived states (\circ) obtained from the $h\nu = 80$ eV and $h\nu = 130$ eV valence bands in Fig. 5 and by using (2), as described in the text. Their sum (\bullet) represents the total DOS of the d -character in $i\text{-Al}_{65}\text{Cu}_{20}\text{Os}_{15}$

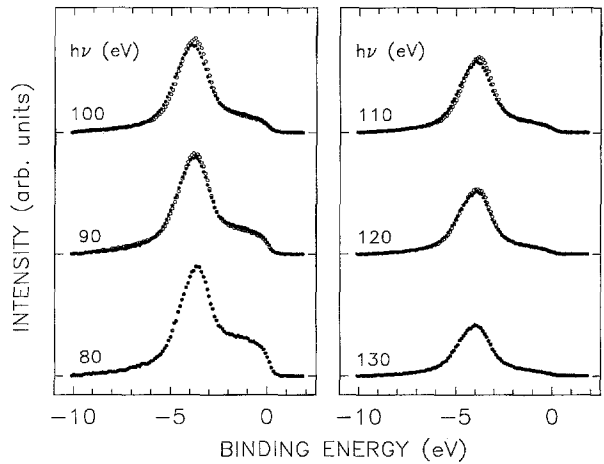


Fig. 9. Comparison of the valence bands generated from (2) by using the empirical partial Cu 3d and Os 5d DOS from Fig. 8 (\bullet) with the experimental valence bands from Fig. 5 (\circ)

cipate that the contribution of the Os 5d-like states to the $\text{DOS}(E_F)$ is not negligible. The Al sp states are expected to spread throughout the valence band (Fig. 10), but cannot be detected clearly in the measured spectra due to the small σ values associated with the Al s and p orbitals (Fig. 2). As mentioned before, the Al sp -derived states are manifested as a broad spectral weight around $\text{BE} = -6$ eV where the contributions from the Cu 3d- and Os 5d-derived states are relatively small.

When the valence band of $i\text{-Al}_{65}\text{Cu}_{20}\text{Os}_{15}$ is compared with the valence bands of two other thermodynamically stable i -alloys, $\text{Al}_{65}\text{Cu}_{20}\text{Ru}_{15}$ and $\text{Al}_{65}\text{Cu}_{20}\text{Fe}_{15}$ (Fig. 11), two common characteristics stand out. Firstly, the Cu 3d-derived features are pushed away from E_F in comparison to their locations in a pure Cu metal, whereas the features associated with the Os 5d-, Ru 4d-, and Fe 3d-derived states remain close to E_F . Thus one would expect a relatively small contribution to the $\text{DOS}(E_F)$

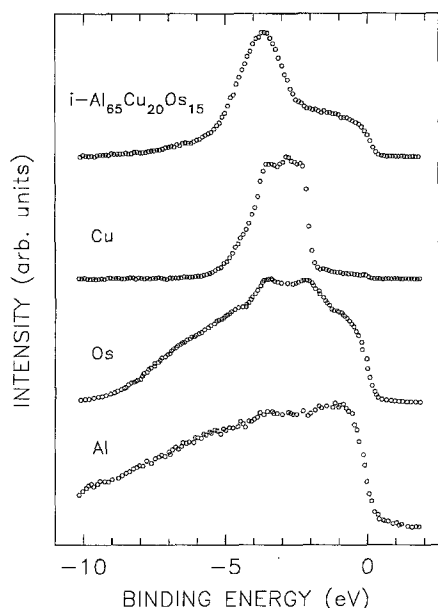


Fig. 10. Comparison of the PES valence band of $i\text{-Al}_{65}\text{Cu}_{20}\text{Os}_{15}$ with that of Cu metal (the raw PES spectrum of Cu was kindly provided by Drs. T.-U. Nahm and S.-J. Oh; the secondary-electron contribution was subtracted from the original spectrum), and with the Al and Mg $K\alpha$ XPS valence bands of Os and Al metals obtained respectively from Fig. 3b of [74] and Fig. 2 [75]. The first two valence bands were measured at $h\nu = 80$ eV. The spectra were normalized to give a constant height between the maximum and minimum recorded count

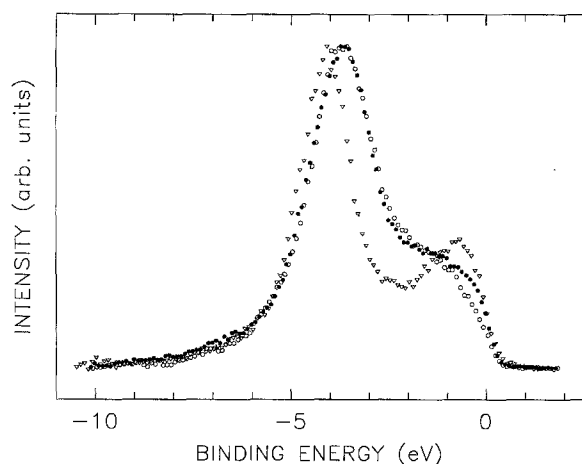


Fig. 11. Valence bands of $i\text{-Al}_{65}\text{Cu}_{20}\text{Os}_{15}$ (\bullet), $i\text{-Al}_{65}\text{Cu}_{20}\text{Ru}_{15}$ (\circ), and $i\text{-Al}_{65}\text{Cu}_{20}\text{Fe}_{10}$ (∇) measured respectively at $h\nu = 80, 90$ and 100 eV. The raw spectrum of $i\text{-Al}_{65}\text{Cu}_{20}\text{Fe}_{15}$ from [48] has been corrected for the energy dependence of the electron transmission of the electron-energy analyzer, normalized for the photon flux, and corrected for the secondary-electron background. The spectrum of $i\text{-Al}_{65}\text{Cu}_{20}\text{Ru}_{15}$ is from [50]. The spectra were normalized to give a constant height between the maximum and minimum recorded count

from the Cu 3d-like states and a non-negligible, although also small, contribution due to the Os 5d-, Ru 4d-, and Fe 3d-like states (Fig. 11). Secondly, there is a strong reduction of the PES intensity as the energy approaches E_F .

The decrease of intensity as the energy approaches E_F which has been observed in the PES [42, 43, 48, 49, 52–54] and SXE [44–47, 51, 52, 54] spectra of the QCs containing TM elements, and is also observed here (Figs. 1, 3, 5, 7, 8), has been interpreted as evidence for the opening of a theoretically predicted [22–32] pseudogap at E_F . Such an interpretation, however, is open to criticism because, as noted earlier [43, 50, 55], there is an alternate interpretation which would lead to the intensity decrease as the energy approaches E_F . It invokes a simple Fermi cut-off, which would be especially important for the QCs with TM elements whose d -states, as was demonstrated in this work, contribute to the measured intensity around E_F . In the case of the studied $i\text{-Al}_{65}\text{Cu}_{20}\text{Os}_{15}$, the Os 5d-derived states do contribute to the measured intensity at E_F (Figs. 7 and 8). We are only able to conclude that our PES results are indicative of a possible opening of a pseudogap at E_F in $i\text{-Al}_{65}\text{Cu}_{20}\text{Os}_{15}$, but they do not prove its existence.

The PES experiments performed so far on QCs had an energy resolution, which is dependent on the photon energy used, between 0.3 and 0.7 eV, with the exception of one PES study conducted with the claimed energy resolution of 0.14 eV [42]. The only IPES study reported so far had an energy resolution of 0.7 eV [43]. The SXE and SXA studies previously reported had an energy resolution, which is dependent on the element considered, in the range 0.2–0.7 eV, and a relatively high uncertainty (0.1–0.3 eV) associated with the determination of the position of E_F . We suggest that these energy resolutions are not high enough, and in the case of the SXE/SXA studies, the uncertainty in determining the location of E_F is too large and the lifetime broadening effects too severe, to warrant the claims of a definite spectroscopic verification of the existence of a pseudogap at E_F . As we shall argue below, high energy-resolution PES/IPES and/or SXE/SXA experiments are essential for obtaining convincing experimental evidence for the possible existence of such a pseudogap.

To illustrate the importance of high energy-resolution for deriving meaningful conclusions from the PES/IPES and SXE/SXA spectroscopic studies of QCs and the limitations imposed by the lifetime broadening effects inherent in these spectroscopic techniques, we make use of the theoretical DOS (kindly provided to us by T. Fujiwara) which was calculated for the hypothetical cubic $\text{Al}_{114}\text{Mn}_{24}$ alloy representing the 1/1 approximant $\alpha\text{-Al-Mn-Si}$ of the $i\text{-Al-Mn-Si}$ alloys [27]. In order to compare this theoretical DOS with an XPS experiment employing the monochromatized Al $K\alpha$ radiation (1486.6 eV), the theoretical partial Al and Mn DOS corresponding to different orbital angular momenta [27] were multiplied by the corresponding σ values [65] per electron and their sum representing the theoretical XPS valence band of an $i\text{-Al-Mn}$ alloy is shown in Fig. 12. The theoretical XPS valence band (Fig. 12) is very similar to the original total DOS [27]; the only difference is the partial suppression of the Al sp feature in the theoretical XPS spectrum caused by the much smaller σ_{Al} values than the corresponding σ_{Mn} values [65]. The main characteristic of this theoretical XPS spectrum is the presence of a major, wide pseudogap whose centre is located at about 0.31 eV above E_F (inset in

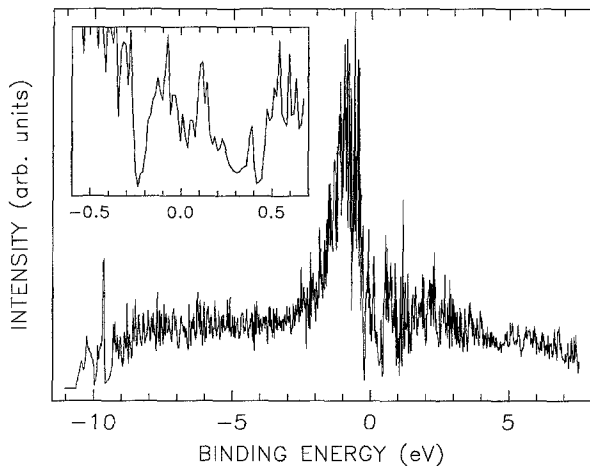


Fig. 12 Theoretical Al $K\alpha$ XPS valence band for the 1/1 approximant α -Al-Mn-Si of the *i*-Al-Mn-Si alloys calculated on the basis of the theoretical DOS from [27], as explained in the text. The inset shows a part of this band around E_F

Fig. 12 and Ref. 27). Defining the width (in terms of FWHM) of this gap is somewhat arbitrary, but it may be considered to extend from $BE = 0.15$ eV to $BE = 0.47$ eV, i.e., its width is 0.32 eV. It is obvious that this major pseudogap cannot be found with PES/XPS experiments which probe the occupied electronic states below E_F . There are two additional, narrower pseudogaps in the theoretical XPS spectrum of an *i*-Al-Mn alloy (Fig. 12): one located at about $BE = -0.24$ eV and the other at about $BE = 0.04$ eV. The values of their FWHM are respectively 0.10 and 0.11 eV. This means that unless the energy resolution of a PES/XPS experiment is better than 0.1 eV, the presence of these pseudogaps cannot be detected.

The additional difficulty in an unambiguous interpretation of the PES(XPS)/IPES and SXE/SXA spectra in relation to the theoretical DOS is caused by lifetime broadening effects which are inherent to these techniques. They smear out the subtle DOS features and therefore should be taken into account. These effects are especially severe for the SXE and SXA techniques. Figure 13 shows the theoretical XPS spectrum from Fig. 12 which has been first multiplied by the Fermi-Dirac distribution function at room temperature, then convoluted with a Lorentzian, to account for the lifetime broadening, and with a Gaussian, to account for the instrumental broadening. The Lorentzian FWHM was taken in the form $\Gamma_L^0 (|BE| - E_F)^2$ [76]. The Γ_L^0 parameter, which fixes the scale of the broadening, was chosen to be equal to 0.05 eV $^{-1}$ and is a typical value used for other metallic systems [73, 76]. It is also compatible with the experimental XPS valence band data presented below. The FWHM of the Gaussian, Γ_G , was varied from 0.02 eV, which is close to the best energy resolution which can be achieved at present [77], to 0.6 eV, which corresponds to a typical PES/XPS resolution (Fig. 13). Since the two pseudogaps located below E_F are very narrow (Fig. 12), they induce a very sharp drop of the spectral weight just before E_F which can be detected only by using a PES measurement with an energy resolution better than 0.1 eV. A comparison (Fig. 14) of the Al $K\alpha$ XPS valence band of the *i*-Al $_{72.5}$ Mn $_{17.4}$ Si $_{10.1}$

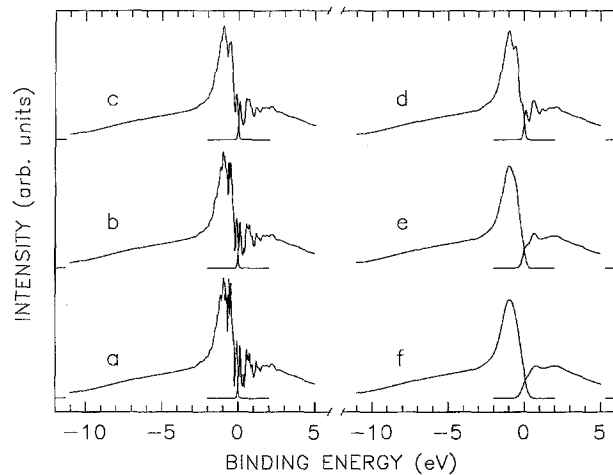


Fig. 13. Theoretical XPS spectrum from Fig. 12 multiplied by the Fermi-Dirac distribution function at room temperature and convoluted with a Lorentzian of the FWHM equal to $\Gamma_L^0 (|BE| - E_F)^2$, where $\Gamma_L^0 = 0.05$ eV $^{-1}$, and with a Gaussian of the FWHM equal to (a) 0.02 eV, (b) 0.05 eV, (c) 0.1 eV, (d) 0.2 eV, (e) 0.4 eV, and (f) 0.6 eV, as explained in the text

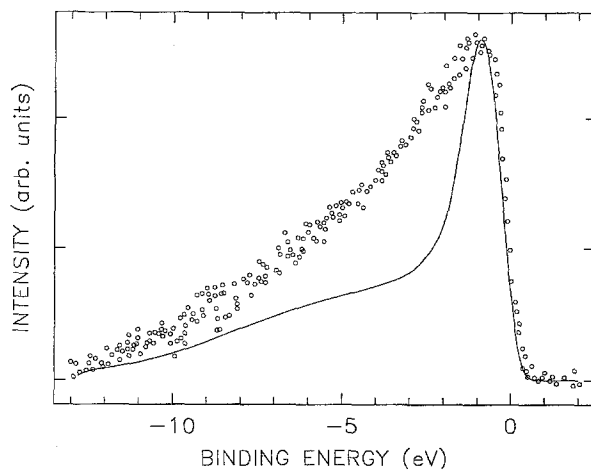


Fig. 14. Comparison between an Al $K\alpha$ valence band of *i*-Al $_{72.5}$ Mn $_{17.4}$ Si $_{10.1}$ from [52], from which the contribution of the impurity peak at $BE = -10$ eV and the secondary-electron contribution were subtracted, with the theoretical XPS spectrum from Fig. 12 which was first multiplied by the Fermi-Dirac distribution function at room temperature, then Lorentzian broadened with $\Gamma_L^0 = 0.05$ eV $^{-1}$ and Gaussian broadened with $\Gamma_G = 0.6$ eV

alloy [52] with the Lorentzian and Gaussian broadened theoretical XPS spectrum from Fig. 12 shows a very poor agreement. There is a very large experimental spectral weight which cannot be accounted for by theory, and which is most probably due to a severe surface contamination of the studied sample [52]. It is impossible to conclude anything meaningful about the existence of a pseudogap from the intensity decrease in the vicinity of E_F in the XPS spectrum shown in Fig. 14.

The theoretical Al 3p partial DOS of the *i*-Al-Mn-Si alloys (Fig. 15) also exhibits several pseudogaps. The major one is again above E_F , and thus cannot be probed with the SXE technique. The other two are located at about $BE = -0.24$ eV and 0.04 eV. Their approximate

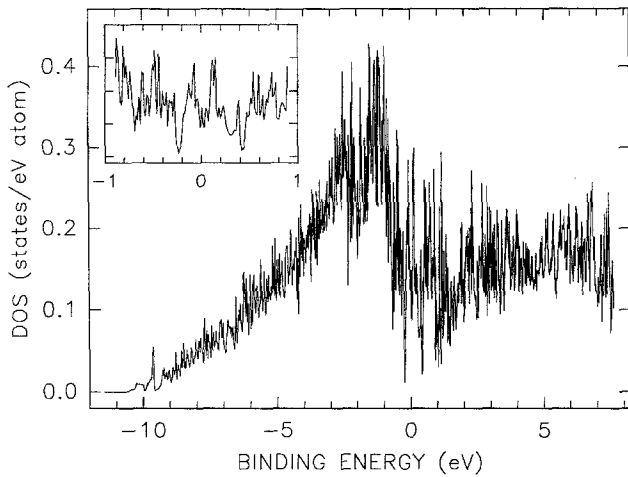


Fig. 15. Al 3p DOS for the 1/1 approximant α -Al-Mn-Si of the i -Al-Mn-Si alloys [27]. The inset shows a part of the DOS around E_F

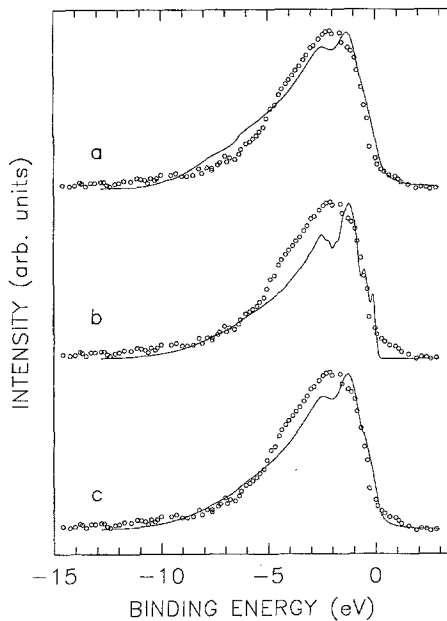


Fig. 16. DOS from Fig. 15 which was first multiplied by the Fermi-Dirac distribution function at room temperature, and then convoluted with a Lorentzian in the form $\Gamma_F + \Gamma_L^0(|BE| - E_F)^2$, where (a) $\Gamma_F = 0.5$ eV and $\Gamma_L^0 = 0.0$ eV $^{-1}$, (b) $\Gamma_F = 0.0$ eV, $\Gamma_L^0 = 0.02$ eV $^{-1}$, and (c) $\Gamma_F = 0.30$ eV and $\Gamma_L^0 = 0.02$ eV $^{-1}$, and with a Gaussian of the FWHM equal to 0.2 eV. The convoluted DOS is shown as a solid line and the experimental Al K β SXE spectrum of i -Al $_{72.5}$ Mn $_{17.4}$ Si $_{10.1}$ from [52] is plotted with open circles

FWHM values are respectively 0.11 eV and 0.15 eV. In Fig. 16 a comparison is made between the experimental Al K β SXE spectrum of i -Al $_{72.5}$ Mn $_{17.4}$ Si $_{10.1}$ from [52] and the Al 3p DOS from Fig. 15. The latter was multiplied by the Fermi-Dirac distribution function at room temperature and broadened to account for lifetime and instrumental broadening effects. The Gaussian FWHM was set to 0.2 eV, which is the value given in the previous SXE studies [41, 45]. The Lorentzian FWHM was assumed to

have the form $\Gamma_F + \Gamma_L^0(|BE| - E_F)^2$ allowing for the possibility of broadening also at E_F . In some SXE studies [78] the Lorentzian broadening (FWHM) is assumed to be constant throughout the SXE spectrum ($\Gamma_L^0 = 0$). However, this leads to poor agreement between the experimental Al K β SXE spectrum and the Al 3p DOS from Fig. 15 when it has been broadened using the parameters from [78] (Fig. 16a). This confirms the assumption made in the majority of spectroscopic studies that Lorentzian broadening is well described by a linear or quadratic dependence on $(|BE| - E_F)$ [73, 76, 79, 80]. The Lorentzian broadening which does not allow for broadening at E_F (Fig. 16b) also results in a poor agreement. A moderate agreement (Fig. 16c) was obtained with $\Gamma_F = 0.3$ eV and $\Gamma_L^0 = 0.02$ eV $^{-1}$; these parameters are close to the typical values used for other alloy systems [79, 80]. It is clear from Fig. 16c that the lifetime broadening effects are too severe to make any meaningful inference about the possible existence of the pseudogaps shown in Fig. 15. Yet it was concluded from the broad and structureless Al K β SXE spectra of i -Al $_{72.5}$ Mn $_{17.4}$ Si $_{10.1}$ and of pure Al that a pseudogap of the width 0.45(5) eV does exist in i -Al $_{72.5}$ Mn $_{17.4}$ Si $_{10.1}$ [52].

The above analysis shows that the interpretation of the low energy-resolution spectroscopic data [41–47, 49, 51–54] almost exclusively in terms of the Hume-Rothery mechanism is unfounded. The explanation for the enormous popularity of this mechanism [2–4] is beyond the realm of science. We stress that the high energy-resolution PES experiments are essential if we are to verify unambiguously the possible existence of a pseudogap around E_F in QCs. It can be added here that high energy-resolution PES measurements were instrumental in the *direct* observation of the superconducting gap in high- T_c superconductors [81], the pseudogap in the charge-density-wave systems [82], the structure-induced pseudogap in liquid and amorphous alloys [56], the pseudogap in some fullerenes [83], and the metal-insulator transitions in some inorganic compounds [84]. Naturally, the most credible evidence for the possible existence of a pseudogap at E_F in QCs could be obtained by combining the high energy resolution of PES with that of IPES.

As mentioned in the Introduction, the predicted pseudogap around E_F in QCs is a generic, but not a specific property distinguishing QCs from the periodic or aperiodic materials. A property which seems to be specific only to QCs is the spikiness of their DOS [27–30] (Figs. 12 and 15). This spikiness is associated with a large number of non-degenerated flat bands in QCs and the presence of TM elements in QCs results in its amplification [30]. The width of a spiky peak is of the order of 0.01–0.02 eV [27–30] (Figs. 12 and 15). The valence bands of i -alloys presented here show no evidence for the presence of such spikes. These spikes have also not been detected in the PES, IPES, SXE, or SXA experiments performed so far [39–55]. There are at least two possible explanations of the failure to detect those spikes experimentally. As Figs. 13 and 16 clearly indicate, the spikiness is smeared out completely for typical PES/IPES and SXE/SXA energy resolutions. This spikiness is expected to be preserved, but *only in the vicinity of E_F* , for energy resolutions better than 0.1 eV (Fig. 13). Near E_F , PES and

IPES are certainly the only experimental techniques with a resolution not affected by lifetime broadening which can detect such spikiness. The second explanation invokes the possibility of chemical and topological disorder in QCs of high structural quality, which will be discussed in the next section. Such a disorder can wash out the spikiness of DOS induced by quasiperiodicity. This section concludes with the statement that high energy-resolution (< 0.1 eV) spectroscopic experiments are indispensable for the direct and unambiguous detection of the theoretically predicted pseudogap around E_F and the spikiness of DOS in QCs.

E. Disorder and electronic structure of quasicrystals

As was mentioned in the Introduction, there seems to be a contradiction between the fact that stable, “perfect” (no phason strain) QCs have a high degree of structural perfection and the apparent relevance of the quantum interference theories used to explain some of their electronic transport properties. We suggest one plausible explanation of this apparent contradiction, which may also be relevant to the problem of the experimental observation of DOS spikiness. There are at present 22 known stable QCs: 14 *i*-systems Al-Cu-Li, Mg-Ga-Zn, Al-Cu-(Fe, Ru, Os), Al-Pd-(Mn, Re), and the recently discovered Al-Pd-Mg [85] and Zn-Mg-RE (RE = Y, Gd, Tb, Dy, Ho, Er) [86], and eight decagonal systems Al-Co-(Cu, Ni), Al-Pd-Mn, Al-Rh-(Cu, Ni), and Al-Pd-(Fe, Ru, Os). They are all ternary alloys and 15 of them are based on aluminium. If one envisages that their structure consists of an sp-electron-type sublattice and a d-electron-type sublattice, then clearly one expects the presence of chemical disorder in these sublattices (for example, in the CuFe, CuRu, CuOs, PdMn, PdRe sublattice). Furthermore, the concept of quasiperiodicity implies that no two crystallographic positions of a given atom are exactly the same [87], which can be viewed as a sort of topological disorder. Although these two types of disorder are not seen in the diffraction and electron microscopy experiments on stable QCs, they are clearly detected, but not separated, in other experiments which are more sensitive to the presence of such disorder. For example, local probes such as Mössbauer spectroscopy [88] and NMR [89] clearly detect the presence of a distribution of quadrupole splittings in high-quality stable *i*-alloys. Such a distribution can only exist if there is a chemical and/or topological disorder in the investigated samples. Also the NMR parameters, the Knight shift and the spin-lattice relaxation rate, indicate the presence of some disorder modes [89]. A recent study on the propagation of acoustic shear waves in a single-grain *i*-Al-Pd-Mn alloy shows the similarity of the acoustic properties of this alloy to those of amorphous metals [90]. The results of these experiments [88–90] demonstrate that chemical and/or topological disorder is present also in the high-quality, phason-free, stable *i*-alloys and it must be taken into account in attempts to understand the physical properties of QCs. In particular, this disorder may explain why quantum interference theories are successful in explaining some of the electronic transport properties of stable QCs. It may also wash out the DOS spikiness predicted by the

calculations which are performed for ideal, disorder-free systems.

F. Al 2p chemical shift in Al-based quasicrystals

The Al 2p core level lines in Al metal and in *i*-Al₆₅Cu₂₀Os₁₅ are compared in Fig. 17. It can be noticed that the Al 2p_{1/2} and 2p_{3/2} lines are separated in the Al metal (inset in Fig. 17), but they overlap in the *i*-Al₆₅Cu₂₀Os₁₅ alloy. The separation of the Al 2p_{1/2} and 2p_{3/2} lines in the Al metal determined from a fit using the two Doniach-Šunjić [91] profiles convoluted with a Gaussian (inset in Fig. 17) is 0.41 (1) eV, which is in a good agreement with the value of 0.42 eV reported in the literature [92]. The Gaussian FWHM obtained from the fit was 0.418(7) eV. This, together with the observation of the Al 2p_{1/2} and 2p_{3/2} components in the Al metal, confirms that the overall energy resolution of the measured PES spectra is 0.4 eV. The main result obtained from Fig. 17 is the observation of a BE shift in *i*-Al₆₅Cu₂₀Os₁₅ by 0.11(3) eV towards lower absolute BE values with respect to Al metal.

There are only a few reports of shifts of the core-level lines in QCs with respect to pure elements and/or to other crystalline alloys. Ederer et al. [39] reported the chemical shifts of 0.2 eV between the Al-Mn alloys of different crystal structure and pure Al, and of less than 0.1 eV between the Al-Mn alloys of crystalline and icosahedral structure. Matsubara et al. [43] found a 0.4 eV shift of the Al 2p and Li 1s lines towards higher absolute BE values in *i*-Al₅₅Li_{35.8}Cu_{9.2} with respect to the Frank-Kasper crystalline alloy Al₅₄Li_{36.8}Cu_{9.2}. The absolute BE shift of the Al 2p line in *i*-Al₇₀Pd₂₀Mn₁₀ with respect to a pure Al metal reported by Zhang et al. [50] was 0.27(10) eV. The values of the observed shifts are small and are comparable to those observed in crystalline alloys [93]. The interpretation of the BE shift is complicated by the fact that it consists of contributions due to chemical, configuration, and relax-

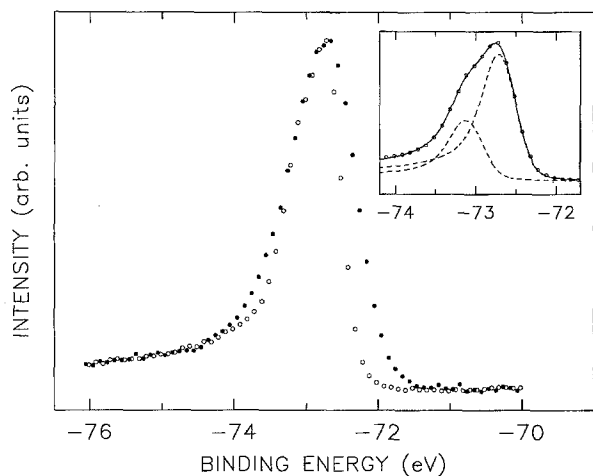


Fig. 17. Al 2p photoemission spectra of the Al metal (○) and the *i*-Al₆₅Cu₂₀Os₁₅ alloy (●) measured at $h\nu = 100$ eV. The spectra were normalized to give a constant height between the maximum and minimum recorded count. The inset shows the fit (solid line) of the Al 2p spectrum of the Al metal with two Doniach-Šunjić profiles convoluted with a Gaussian, which are shown with a broken line, corresponding to Al 2p_{1/2} and 2p_{3/2} core levels

ation shifts [94]. These contributions are difficult to evaluate theoretically even for simple binary alloys [94].

4. Conclusions

The structure of the valence band of *i*-Al₆₅Cu₂₀Os₁₅ consists of two main features with the maximum intensity at 1.5(1) and 3.7(1) eV below E_F . The first feature was shown to be due mainly to the Os 5d-derived state, whereas the other was demonstrated to result from the states of a predominantly Cu 3d character. The Os 5d and Cu 3d partial density of states were determined empirically from the measured valence bands. It was shown that the density of states of each of these two elements is distributed throughout the width of the band. The decrease of intensity as the energy approaches E_F was interpreted as indicative of the presence of a minimum in the DOS around E_F . It was indicated, however, that the Fermi cut-off also contributes to the observed intensity decrease. It was demonstrated that high energy-resolution experiments probing the DOS below and above E_F are essential to unambiguously determine the possible presence of such a pseudogap in quasicrystals. Presently available spectroscopic data have insufficiently high energy-resolution to convincingly demonstrate the presence of such a pseudogap. The spikiness of the density of states predicted by theory was not observed within the energy resolution of the experiment. It was shown that such a spikiness can be detected unambiguously in the vicinity of E_F only by PES/IPES techniques using the highest available energy resolution. A review of the current status of the electronic structure studies of icosahedral alloys was also presented.

This work was supported by the Natural Sciences and Engineering Research Council of Canada, a Grant-in-Aid for Scientific Research from the Ministry of Education, Science, and Culture of Japan, and the Iketani Science and Technology Foundation. The research was carried out (in part) at the National Synchrotron Light Source, Brookhaven National Laboratory, which is supported by the U.S. Department of Energy, Division of Materials Sciences and Division of Chemical Sciences (DOE contract number DE-AC02-76CH00016). Two of us (ZMS and GWZ) are indebted to Dr. M.-L. Shek for her help in conducting the PES experiments and to Prof. T. Fujiwara for providing the DOS of the approximant of the *i*-Al-Mn-Si alloys.

References

- Schechtman, D., Blech, I., Gratias, D., Cahn, J.W.: Phys. Rev. Lett **53**, 1951 (1984)
- For a review, see Janot, C.: Quasicrystals, a primer. Oxford: Clarendon Press 1992
- For reviews, see Quasicrystals, the state of the art. DiVincenzo, D.P., Steinhardt, P.J. (eds.) Singapore: World Scientific 1991; Quasicrystals. Fujiwara, T., Ogawa, T. (eds.), Berlin, Heidelberg, New York: Springer 1990
- For a review, see Poon, S.J.: Adv. Phys. **41**, 303 (1992)
- O'Handley, R.C., Dunlap, R.A., McHenry, M.E.: In: Handbook of Magnetic Materials, Vol. 6, p. 453. Buschow, K.H.J. (ed.), Amsterdam, London, New York: North-Holland 1991
- Stadnik Z.M., Stroink, G.: Phys. Rev. **B43**, 894 (1991); Phys. Rev. **B44**, 4255 (1991)
- Nasu S., Miglierini, M., Kuwano, T.: Phys. Rev. **B45**, 12778 (1992)
- Tsai, A.-P., Inoue, A., Masumoto, T.: Jpn. J. Appl. Phys. **26**, L1505 (1987)
- Tsai, A.-P., Inoue, A., Masumoto, T.: Jpn. J. Appl. Phys. **27**, L1587 (1988)
- Tsai, A.P., Inoue, A., Yokoyama, Y., Masumoto, T.: Mater. Trans., Jpn. Inst. Metals **31**, 98 (1990); Phil. Mag. Lett. **61**, 9 (1990)
- Tsai, A.-P., Yokoyama, Y., Inoue, A., Masumoto, T.: Jpn. J. Appl. Phys. **29**, L1161 (1990)
- Honda, Y., Edagawa, K., Yoshioka, A., Hashimoto, T., Takeuchi, S.: Jpn. J. Appl. Phys. **A33**, 4929 (1994)
- Mott, N.: Conduction in non-crystalline materials. Oxford: Clarendon Press 1993
- Pierce, F.S., Poon, S.J., Guo, Q.: Science **261**, 737 (1993)
- Klein, T., Berger, C., Mayou, D., Cyrot-Lackmann, F.: Phys. Rev. Lett. **66**, 2907 (1991)
- Berger, C., Grenet, T., Lindqvist, P., Lanco, P., Grieco, J.C., Fourcaudot, G., Cyrot-Lackmann, F.: Solid State Commun. **87**, 977 (1993)
- Matsuo, S., Ishimasa, T., Nakano, H., Fukano, Y.: J. Phys. **F18**, L175 (1988); Stadnik, Z.M., Stroink, G., Ma, H., Williams, G.: Phys. Rev. **B39**, 9797 (1989)
- Hume-Rothery, W.: J. Inst. Metals **35**, 295 (1926); The metallic state. London, Edinburgh, Glasgow: Oxford University Press 1931
- Mott, N.F., Jones, H.: The theory of the properties of metals and alloys. Glasgow, New York, Toronto: Oxford University Press 1958
- Phillips, J.C.: Phys. Rev. **B47**, 7747 (1993)
- Heine, V., Weaire, D.: In: Solid state physics. Advances in Research and Applications, Vol. 24, p. 249. Ehrenreich, H., Seitz, F., Turnbull, D. (eds.) New York, London: Academic Press 1970; Cottrell, A.: Introduction to the modern theory of metals. London: The Institute of Metals 1988
- Smith, A.P., Ashcroft, N.W.: Phys. Rev. Lett. **59**, 1365 (1987)
- Friedel, J., Dénoyer, F.: C.R. Acad. Sci. (Paris) **305**, 171 (1987); Friedel, J.: Helv. Phys. Acta **61**, 538 (1988); Phil. Mag. **B65**, 1125 (1992)
- Vaks, V.G., Kamysenko, V.V., Samolyuk, G.D.: Phys. Lett. **A132**, 131 (1988)
- Fradkin, M.A.: J. Phys.: Condensed Matter **4**, 10497 (1992)
- Carlsson, A.E.: Phys. Rev. **B47**, 2515 (1993); J. Non-Cryst. Solids **153** & **154**, 386 (1993)
- Fujiwara, T.: Phys. Rev. **B40**, 942 (1989); J. Non-Cryst. Solids **117** & **118**, 844 (1990); Fujiwara, T., Trambly de Laissardière, G., Yamamoto, S.: Mater. Sci. Eng. **A179** & **180**, 118 (1994)
- Fujiwara, T., Yokokawa, T.: Phys. Rev. Lett. **66**, 333 (1991); Fujiwara, T.: J. Non-Cryst. Solids **153** & **154**, 390 (1993)
- Fujiwara, T., Yamamoto, S., Trambly de Laissardière, G.: Phys. Rev. Lett. **71**, 4166 (1993); Fujiwara, T.: J. Non-Cryst. Solids **156** & **158**, 865 (1993); Mater. Sci. Eng. **B19**, 77 (1993)
- Trambly de Laissardière, G., Fujiwara, T.: Phys. Rev. **B50**, 5999 (1994)
- Hafner, J., Krajčí, M.: Phys. Rev. Lett. **68**, 2321 (1992); Europhys. Lett. **17**, 145 (1992); J. Non-Cryst. Solids **150**, 337 (1992)
- Hafner, J., Krajčí, M.: Phys. Rev. **B47**, 11795 (1993)
- Hippert, F., Kandel, L., Calvayrac, Y., Dubost, B.: Phys. Rev. Lett. **69**, 2086 (1992)
- Phillips, J.C., Rabe, K.M.: Phys. Rev. Lett. **66**, 923 (1991)
- Phillips, J.C.: Solid State. Commun. **83**, 379 (1992); Phys. Rev. **B47**, 2522 (1993); Phys. Rev. **B47**, 7747 (1993)
- Mayou, D., Berger, C., Cyrot-Lackmann, F., Klein, T., Lanco, P.: Phys. Rev. Lett. **70**, 3815 (1993)
- Yamamoto, S., Fujiwara, T.: Mater. Sci. Eng. **A181** & **182**, 726 (1994)
- Chernikov, M.A., Bernasconi, A., Beeli, C., Ott, H.R.: Europhys. Lett. **21**, 767 (1993)
- Bruhwyler, P.A., Shen, Y., Schnatterly, S.E., Poon, S.J.: Phys. Rev. **B36**, 7347 (1987); Bruhwyler, P.A., Wagner, J.L., Biggs, B.D., Shen, Y., Wong, K.M., Schnatterly, S.E., Poon, S.J.: Phys. Rev. **B37**, 6529 (1988); Ederer, D.L., Schaefer, R., Tsang, K.-L., Zhang, C.H., Callcott, T.A., Arakawa, E.T.: Phys. Rev. **B37**, 8594 (1988)
- Traverse, A., Dumoulin, L., Belin, E.: In: Quasicrystalline materials, p. 399. Janot, Ch., Dubois, J.M. (eds.) Singapore: World Scientific 1988
- Belin, E., Traverse, A.: J. Phys.: Condensed Matter **3**, 2157 (1991)

42. Mori, M., Matsuo, S., Ishimasa, T., Matsuura, T., Kamiya, K., Inokuchi, H., Matsukawa, T., *J. Phys.: Condensed Matter* **3**, 767 (1991); Mori, M., Kamiya, K., Matsuo, S., Ishimasa, T., Nakano, H., Fujimoto, H., Inokuchi, H.: *J. Phys.: Condensed Matter* **4**, L157 (1992)
43. Matsubara, H., Ogawa, S., Kinoshita, T., Kishi, K., Takeuchi, S., Kimura, K., Suga, S., *Jpn. J. Appl. Phys.* **A30**, L389 (1991)
44. Belin, E., Kojnok, J., Sadoc, A., Traverse, A., Harmelin, M., Berger, C., Dubois, J.-M.: *J. Phys.: Condensed Matter* **4**, 1057 (1992)
45. Belin, E., Dankhazi, Z., Sadoc, A., Calvayrac, Y., Klein, T., Dubois, J.-M.: *J. Phys.: Condensed Matter* **4**, 4459 (1992)
46. Belin, E.: In *Physics and Chemistry of Finite Systems*, Vol. II, p. 829. Jena, P., Khanna, S.N., Rao, B.K. (eds) Amsterdam: Kluwer 1992
47. Belin, E., Danhakazi, Z.: *J. Non-Cryst. Solids* **153** & **154**, 298 (1993); Sadoc, A., Belin, E., Dankhazi, Z., Flank, A.M.: *J. Non-Cryst. Solids* **153** & **154**, 338 (1993); Belin, E., Dankhazi, Z., Sadoc, A., *J. Non-Cryst. Solids* **156** & **158**, 896 (1993); Belin, E., Mayou, D., *Phys. Scr.* **T49**, 356 (1993); Berger, C., Belin, E., Mayou, D.: *Ann. Chim. Fr.* **18**, 485 (1993); Belin, E., Traverse, A., Sonder, A.: *Nucl. Instrum. Methods Phys. Res.* **B80** & **81**, 80 (1993)
48. Stadnik, Z.M., Stroink, G.: *Phys. Rev.* **B47**, 100 (1993); *J. Non-Cryst. Solids* **156** & **158**, 891 (1993)
49. Mizutani, U., Matsuda, T., Itoh, Y., Tanaka, K., Domae, H., Mizuno, T., Murasaki, S., Miyoshi, Y., Hashimoto, K., Yamada, Y.: *J. Non-Cryst. Solids* **156** & **158**, 882 (1993)
50. Zhang, G.W., Stadnik, Z.M., Tsai, A.-P., Inoue, A.: *Phys. Lett.* **A186**, 345 (1994); *Phys. Rev.* **B50**, 6696 (1994)
51. Belin, E., Dankhazi, Z., Sadoc, A.: *Mater. Sci. Eng.* **A181** & **182**, 717 (1994)
52. Belin, E., Miyoushi, Y., Yamada, Y., Ishikawa, T., Matsuda, T., Mizutani, U.: *Mater. Sci. Eng.* **A181** & **182**, 730 (1994)
53. Nakamura, Y., Mizutani, U.: *Mater. Sci. Eng.* **A181** & **182**, 790 (1994)
54. Hashimoto, K., Yamada, Y., Yamauchi, T., Tanaka, T., Matsuda, T., Mizutani, U.: *Mater. Sci. Eng.* **A181** & **182**, 785 (1994); Mizutani, U., Yamada, Y., Takeuchi, T., Hashimoto, K., Belin, E., Sadoc, A., Yamauchi, T., Matsuda, T.: *J. Phys.: Condensed Matter* **6**, 7335 (1994)
55. Stadnik, Z.M., Zhang, G.W., Tsai, A.-P., Inoue, A.: *J. Phys.: Condensed Matter* **6**, 6885 (1994)
56. Häussler, P.: *Phys. Rep.* **222**, 65 (1992)
57. McHenry, M.E., Eberhart, M.E., O'Handley, R.C., Johnson, K.H.: *Phys. Rev. Lett.* **56**, 81 (1986)
58. De Coulon, V., Reuse, F.A., Khanna, S.N.: *Phys. Rev.* **B48**, 814 (1993); Liu, F., Khanna, S.N., Magaud, L., Jena, P., De Coulon, V., He, X.-G., Cyrot-Lackmann, F.: *Phys. Rev.* **B48**, 1295 (1993)
59. Tsai, A.-P., Inoue, A., Nasumoto, T.: *Mater. Trans. Jpn. Inst. Metals* **30**, 666 (1989)
60. Matsubara, E., Waseda, Y.: In: *Quasicrystals*, p. 96. Kuo, K.H., Ninomiya, T. (eds). Singapore: World Scientific 1991
61. Shinohara, T., Tsai, A.P., Sato, T., Masumoto, T.: *J. Mater. Res.* **7**, 1970 (1992)
62. Stadnik, Z.M., Zhang, G.W., Tsai, A.-P., Inoue, A.: (to be published)
63. Helmer, J.C., Weichert, N.H.: *Appl. Phys. Lett.* **13**, 266 (1968)
64. Shirley, D.A., *Phys. Rev.* **B5**, 4709 (1972)
65. Yeh, J.-J.: *Atomic calculation of photoionization cross-sections and asymmetry parameters*. London: Gordon and Breach 1993
66. Allen, J.W.: In: *Synchrotron radiation research. Advances in Surfaces and Interface Science*, Vol. 1, p. 253. Bachrach, R.Z. (ed.), New York, London: Plenum Press 1992
67. Fuggle J.C., Mårtensson, N.: *J. Electr. Spectrosc. Relat. Phenom.* **21**, 275 (1980)
68. Rossi, G., Lindau, I., Braicovich, L., Abbati, I.: *Phys. Rev.* **B28**, 3031 (1983); Cole, R.J., Evans, J.A., Duò, L., Laine, A.D., Fowles, P.S., Weightman, P., Mondio, G., Norman, D.: *Phys. Rev.* **B46**, 3747 (1992)
69. Davis, L.C.: *J. Appl. Phys.* **59**, R25 (1986); Kunz, C.: In: *Photoemission in Solids II*, p. 299. Ley, L., Cardona, M. (eds.), Berlin Heidelberg, New York: Springer 1979
70. Eastman, D.E., Grobman, W.D.: *Phys. Rev. Lett.* **28**, 1327 (1972); Freouf, J., Erbudak, M., Eastman, D.E.: *Solid State Commun.* **13**, 771 (1973); Feibelman, P.J., Eastman, D.E.: *Phys. Rev.* **B10**, 4932 (1974); Nahm, T.-U., Han, M., Oh, S.-J., Park, J.-H., Allen, J.W., Chung, S.-M.: *Phys. Rev. Lett.* **70**, 3663 (1993)
71. Wright, H., Weightman, P., Andrews, P.T., Folkerts, W., Flipse, C.F.J., Sawatzky, G., Norman, D., Padmore, H.: *Phys. Rev.* **B35**, 519 (1987)
72. Folkerts, W., Van Der Marel, D., Haas, C., Sawatzky, G.A., Norman, D., Padmore, H., Wright, H., Weightman, P.: *J. Phys.* **F17**, 657 (1987)
73. Allen, J.W., Oh, S.J., Gunnarsson, O., Schönhammer, K., Maple M.B., Torikachvili, M.S., Lindau, I.: *Adv. Phys.* **35**, 275 (1986) Soda, K., Mori, T., Taniguchi, M., Asaoka, S., Naito, K., Ōnuki, Y., Komatsubara, T., Miyahara, T., Sato, S., Ishii, T.: *J. Phys. Soc. Jpn.* **55**, 1709 (1986); Shen, Z.-X., Lindberg, P.A.P., Wells, B.O., Dessau, D.S., Borg, A., Lindau, I., Spicer, W.E., Ellis, W.P., Kwei, G.H., Ott, K.C., Kang, J.-S., Allen, J.W.: *Phys. Rev.* **B40**, 6912 (1989); Weidemann, R., Gumlich, H.-E., Kupsch, M., Middlemann, H.-U., Becker, U.: *Phys. Rev.* **B45**, 1172 (1992); Nohara, S., Namatame, H., Fujimori, A., Takabatake, T.: *Phys. Rev.* **B47**, 1754 (1993); Ueda, Y., Taniguchi, M., Mizokawa, T., Fujimori, A., Souma, I., Oka, Y., *Phys. Rev.* **B49**, 2167 (1994)
74. Nilsson, R., Berndtsson, A., Mårtensson, N., Nyholm, R., Hedman, J.: *Phys. Status Solidi*. (b) **75**, 197 (1976)
75. Baer, Y., Busch, G.: *Phys. Rev. Lett.* **30**, 280 (1973)
76. Höchst, H., Steiner, P., Reiter, G., Hüfner, S.: *Z. Phys.* **B42**, 199 (1981)
77. Patthey, F., Delley, B., Schneider, W.-D., Baer, Y.: *Phys. Rev. Lett.* **55**, 1518 (1985); Weschke, E., Laubschat, C., Simmons, T., Domke, M., Strebel, O., Kaindl, G., *Phys. Rev.* **B44**, 8304 (1991); Hwu, Y., Lozzi, L., La Rosa, S., Onellion, M., Almeras, P., Gozzo, F., Lévy, F., Berger, H., Margaritondo, G.: *Phys. Rev.* **B45**, 5438 (1992)
78. Dankházi, Z., Trambly De Laissardiére, G., Manh, D.N., Belin, E., Mayou, D.: *J. Phys.: Condensed Matter* **5**, 3339 (1993)
79. Weijs, P.J.W., Czyżyk, M.T., Fuggle, J.C., Speier, W., Darma, D.D., Buschow, K.H.J.: *Z. Phys.* **B78**, 423 (1990)
80. Ławniczak-Jabłońska, K., Inoue, J., Tohyama, T., Czyżyk, M.T.: *Phys. Rev.* **B49**, 14165 (1994)
81. Imer, J.-M., Patthey, F., Dardel, B., Schneider, W.-D., Baer, Y., Petroff, Y., Zettl, A.: *Phys. Rev. Lett.* **62**, 336 (1989); Olson, C.G., Liu, R., Yang, A.-B., Lynch, D.W., Arko, A.J., List, R.S., Veal, B.W., Chang, Y.C., Jiang, P.Z., Paulikas, A.P.: *Science* **245**, 731 (1989); Shen, Z.-X., Dessau, D.S., Wells, B.O., King, D.M., Spicer, W.E., Arko, A.J., Marshall, D., Lombardo, L.W., Kapitulnik, A., Dickinson, P., Doniach, S., DiCarlo, J., Loesser, A.G., Park, C.H.: *Phys. Rev. Lett.* **70**, 1553 (1993)
82. Dardel, D., Grioni, M., Malterre, D., Weibel, P., Baer, Y., Lévy, F.: *J. Phys.: Condensed Matter* **5**, 6111 (1993)
83. Takahashi, T.: *Comments Cond. Mat. Phys.* **16**, 113 (1992)
84. Smith, K.E., Henrich, V.E.: *Phys. Rev.* **B50**, 1382 (1994)
85. Koshikawa, N., Sakamoto, S., Edagawa, K., Takeuchi, S.: *Jpn. J. Appl. Phys.* **31**, L966 (1992); Koshikawa, N., Edagawa, K., Takeuchi, S.: *Mater. Trans. Jpn. Inst. Metals* **34**, 188 (1993)
86. Niikura, A., Tsai, A.P., Inoue, A., Masumoto, T.: *Philos. Mag. Lett.* **69**, 351 (1994); Tsai, A.P., Niikura, A., Inoue, A., Masumoto, T., Nishida, Y., Tsuda, K., Tanaka, M.: *Philos. Mag. Lett.* **70**, 169 (1994)
87. Janot, Ch., Dubois, J.M.: *J. Phys.* **F18**, 2303 (1988)
88. Stadnik, Z.M.: *Hyperfine Interact.* **90**, 215 (1994)
89. Shastri, A., Borsa, F., Goldman, A.I., Shield, J.E., Torgeson, D.R.: *J. Non-Cryst. Solids* **153** & **154**, 347 (1993)
90. Vernier, N., Bellessa, G., Perrin, B., Zarembovitch, A., De Boissieu, M.: *Europhys. Lett.* **22**, 187 (1993)
91. Doniach, S., Šunjić, M.: *J. Phys.* **C3**, 285 (1970)
92. Baer, Y., Busch, G., Cohn, P.: *Rev. Sci. Instrum.* **46**, 466 (1975); Flodstrom, S.A., Bachrach, R.Z., Bauer, R.S., Hagström, S.B.: *Phys. Rev. Lett.* **37**, 1282 (1976); Hagström, S.B.M., Bachrach, R.Z., Bauer, R.S., Flodström, S.A.: *Phys. Scr.* **16**, 414 (1977)
93. Hillebrecht, F.U., Fuggle, J.C., Bennett, P.A., Żoźnierek, Z., Freiburg, Ch.: *Phys. Rev.* **B27**, 2179 (1983)
94. Stadnik, Z.M., Stroink, G.: *J. Non-Cryst. Solids* **99**, 233 (1988)